ACS Photonics

pubs.acs.org/journal/apchd5

Letter

Loss-Assisted Metasurface at an Exceptional Point

Shaohua Dong, Guangwei Hu, Qiang Wang, Yuxiang Jia, Qing Zhang, Guangtao Cao, Jiafu Wang, Shuqing Chen, Dianyuan Fan, Weixiang Jiang, Ying Li,* Andrea Alù, and Cheng-Wei Qiu*

Cite This: *ACS Photonics* 2020, 7, 3321−3327

Read Online

ACCESS | Metrics & More | Article Recommendations | Supporting Information

ABSTRACT: Loss in photonic devices is intentionally minimized, as it limits the efficiency and potential functionalities. Here, we report a loss-assisted non-Hermitian electromagnetic metasurface operating at an exceptional point (EP), showing extraordinary angular asymmetry at EP condition. Spatially engineered losses are essential for the exotic scattering response of this metasurface. As a proof of concept, a functional EP metasurface, composed of a judiciously tailored tri-meta-atom supercell, is shown to exhibit unidirectional retro-reflection: totally suppressed reflection when light illuminates from the left, but highly efficient reflection from the right. Our results open promising possibilities for developing new mechanisms and designing functional photonic devices for wave manipulation and fuse exceptional-point physics with flatland optics.

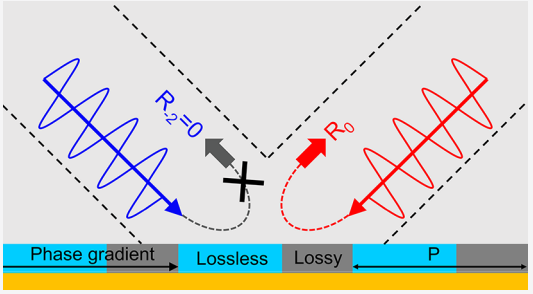

KEYWORDS: *non-Hermitian, metasurface, exceptional point, angular asymmetry*

Electromagnetic metasurfaces, the planarized version of three-dimensional metamaterials, have been investigated as an ultrathin and multifunctional platform that could significantly expand our capabilities to manipulate electromagnetic waves via engineering its microscopic subwavelength unit cells, or so-called meta-atoms.[1,2] Many fascinating properties and applications have thus been achieved, such as anomalous refraction/reflection,[1,3] giant photonic spin Hall effect,[4−6] metalens,[7,8] meta-holograms,[9−11] direction-multiplexed or Janus wavefront control,[12−14] angular-asymmetric absorption,[15,16] surface wave control[17,18] and so on. In general, these functions depend on modulating the real part of the effective dielectric parameters of meta-atoms. However, loss (such as radiation loss, Ohmic loss) is unavoidable, and is usually minimized to enhance efficiency. As recently shown in the exciting context of non-Hermitian physics, as a new degree of freedom is provided by engineering the material response in the entire complex plane of dielectric parameters, paving the way to leveraging loss engineering and modulation for new photonic devices[27−38] and could be key to expanding the functionalities of metasurfaces.[39]

Since complex non-Hermitian Hamiltonians were originally introduced in quantum mechanics,[19−21] the distinctive performance at the parity−time (PT) phase transition point (i.e., exceptional point) has inspired a similar concept in other wave systems, such as optics,[22] acoustics,[23,24] circuits,[25] and even thermal diffusion.[26] It should be noted that exceptional points (EPs), as a more general concept, can be expected in a larger non-Hermitian family.[40−47] In optics, PT-symmetric systems can be realized by considering balanced gain and loss, as illustrated in the left panel of Figure 1(a), where the eigenvalue spectrum can become real.[36,37] Rich physics and appealing applications around EPs have been realized.[27−37] However, it is difficult to realize optical gain, considering the stability of the system, limiting the exploration of EPs for optics and photonics. Thus, all-passive systems without optical gain have been examined and engineered to demonstrate exotic EP-related phenomena. In 2013, Feng et al. demonstrated a 1D all-passive optical waveguide system, showing a unidirectional reflectionless effect sustained by an EP.[38,47] However, such a 1D waveguide system is limited to two port excitations, restricting its applicability in free space. Similar functionalities for free-space radiation may open more opportunities in EP physics. For example, metasurfaces were recently utilized to study EP phenomena in polarization space for free-space radiation.[39,40] Nevertheless, this kind of EP effect is realized in periodic structures and only utilizes 1D propagating channels, which does not fully exploit the potential applications of 2D metasurface systems. Two-dimensional inhomogeneous metasurfaces with multiple channels may provide abundant EP phenomena for various demanding applications, which is still yet to be explored. Besides, there are many inspirational EP physics in other passive non-Hermitian systems.[41−43]

Received: September 16, 2020
Published: December 7, 2020

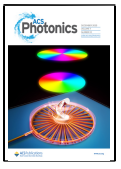

https://dx.doi.org/10.1021/acsphotonics.0c01440
ACS Photonics 2020, 7, 3321−3327

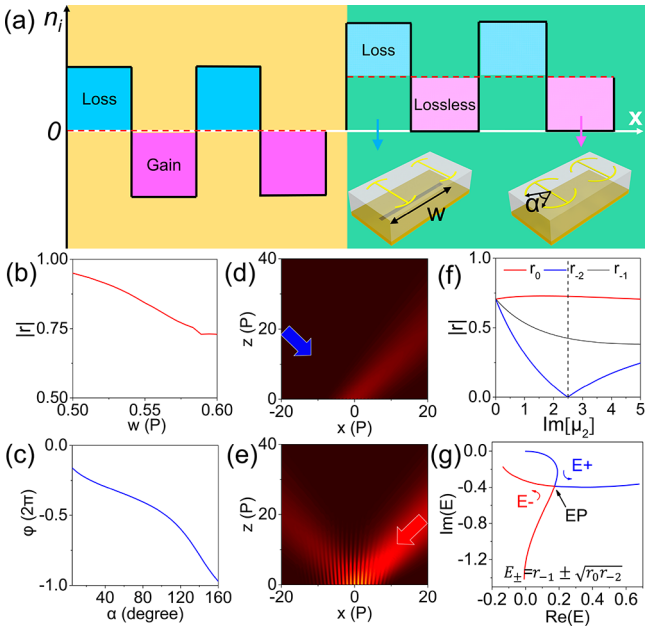

Figure 1. Principle of the non-Hermitian metasurface at the EP. (a) Traditional non-Hermitian system constructed with balanced loss and gain regions (left), while the proposed non-Hermitian metasurface consists of loss and lossless regions (right). The meta-atoms in the lossless region of the non-Hermitian metasurface based on real structures are composed by a dielectric layer sandwiched between the metallic sheet and the metal H-shaped ring layer with opening angle α and a leaky loss introduced into the meta-atoms by a slit in the metal base. (b) Local reflection amplitude versus the length w of the slit at α = 115° for the lossy meta-atom of the non-Hermitian metasurface based on real structures. (c) Local reflection phase versus the opening angle α of the lossless meta-atom of the real non-Hermitian metasurface. The normalized scattering field of the non-Hermitian metasurface [$\varepsilon_1 = 8$, $\varepsilon_2 = \varepsilon_3 = 1$; $\mu_1 = 0.8$, $\mu_2 = 0.5 + i2.49$, $\mu_3 = -3.1$] at the EP for the incident waves from (d) the left-side port and (e) the right-side port, respectively. (f) Extraordinary retro-reflection amplitudes $|r_0|$ and $|r_{-2}|$ and the ordinary specular reflection amplitude $|r_{-1}|$ varying with Im[μ_2] for the EM metasurface. (g) Evolution trajectories of eigenvalues $E_\pm$ of the scattering matrix in the complex plane with the increase of Im[μ_2] (along the directions of the red and blue arrows) for the EM metasurface.

Here, we build a non-Hermitian metasurface by interleaving balanced loss and lossless regions, schematically shown in the right panel of Figure 1(a). The non-Hermitian surface can be constructed by a reflection-type metasurface, in which the meta-atoms are composed by a dielectric layer sandwiched between metallic sheets and metal H-shaped ring layers with opening angle α. The local reflection phase can be arbitrarily modulated by just changing α, as shown in Figure 1(c). Loss can be introduced into the meta-atoms filling loss regions by a slit with length w added in the metal backboard, which realizes a leaky loss for the reflective system. Figure 1(b) intuitively shows how the local reflection amplitude can be modulated by changing w (details shown in Figure 3). As an example of characterizing the EP effect, a two-port phase-gradient metasurface with a lossy modulation is designed to support only two radiative scattering channels of incident waves from two opposite oblique incident angles: an extraordinary retro-reflection and an ordinary specular reflection. The non-Hermitian scattering matrix could thus be derived for this two-port metasurface and exhibits an EP in the complex eigenvalue space thanks to the presence of loss, at which a distinguished Janus scattering feature arises: high-efficiency retro-reflection from the negative incident angle (see Figure 1(e)) and a fully suppressed retro-reflection from the positive one (see Figure 1(d)). Our findings reveal the important potential of realizing non-Hermitian physics in passive metasurfaces via exploiting the loss degree of freedom to enable exotic meta-devices with extreme functionalities.

RESULTS

For a typical reflective phase-gradient metasurface, the deflection angles of different diffraction modes can be determined by momentum conservation:

$$k_{xi} + \xi + mK = k_{xr} \tag{1}$$

Here, $k_{xi} = k_0 \sin\theta_i$ and $k_{xr} = k_0 \sin\theta_r$ are the incident and reflective wavevector components parallel to the metasurface (along the x direction), respectively, k_0 is the free-space wavevector, and θ_i and θ_r correspond to angles of incident and reflected waves (positively valued if the wavevector $k_x > 0$, and negatively valued if vice versa). $\xi = \frac{d\varphi}{dx}$ is the phase gradient along x, i.e., the derivative of the phase with respect to x, and φ is the local phase of the meta-atom as a function of x. $K = 2\pi/P$ is the reciprocal lattice vector induced by the periodicity of metasurface, P is the supercell period of the metasurface, and m (0, ±1, ...) denotes the order of the diffraction channels.

In this work, our two-port surface system is established to possess an extraordinary retro-reflection output port and an ordinary specular reflection output port for incident waves from two input ports, i.e., along the incident angles of ±45°. This gives the diffraction modes of $k_{xr} = \pm k_0/\sqrt{2}$ with fixed incident wave as $k_{xi} = \pm k_0/\sqrt{2}$. To realize such a system, our phase-gradient metasurface is required to satisfy $\xi = 2|k_{xi}|$ and $\xi = K$, according to eq 1. In such a manner, the extraordinary retro-reflection corresponds to $m = -2$ and the ordinary specular reflection gives $m = -1$ when the incident wave comes from the left, i.e., $\theta_i = 45°$ and $k_{xi} = k_0/\sqrt{2}$; the extraordinary retro-reflection fulfills $m = 0$ and the ordinary specular reflection is $m = -1$ when the incident wave comes from the right, i.e., $\theta_i = -45°$ and $k_{xi} = -k_0/\sqrt{2}$. To construct our phase-gradient metasurface, a periodic supercell consisting of three subunits is adopted. On the basis of this two-port framework, we first build an effective medium (EM) model [$\varepsilon = 1$, $\mu(x)$] (where ε and μ represent the effective permittivity and permeability of metasurface, respectively) in parameter space to demonstrate the EP phenomenon at the wavelength λ_0 = 1550 nm (see Sections 1 and 2 of the Supporting Information[3,48]). Although the μ-type metasurface model [$\varepsilon = 1$, $\mu(x)$] is just more suitable for reflection-type metasurface based on sandwich structures like meta-atoms shown in this work,[48] the proposed approach of how to find an EP solution does not depend on the type of EM model in practice. As an example, here the EM metasurface is designed with a 100 nm thickness and backed up with a mirror. The width P of the supercell is about 1096 nm (i. e., $\frac{\lambda_0}{\sqrt{2}}$).

For the two-port system, the total electromagnetic field for each port is the superposition of the incident waves (input) and the scattered waves (output) along the opposite direction $\Psi(\vec{\rho}_{L(R)}) = \Psi_+^{L(R)} e^{-i\vec{k}_0\cdot\vec{\rho}_{L(R)}} + \Psi_-^{L(R)} e^{i\vec{k}_0\cdot\vec{\rho}_{L(R)}}$, where L(R) corresponds to the left (right) port, $\vec{\rho}_{L(R)}$ is the propagating displacement vector of electromagnetic wave along the left

https://dx.doi.org/10.1021/acsphotonics.0c01440
ACS Photonics 2020, 7, 3321−3327

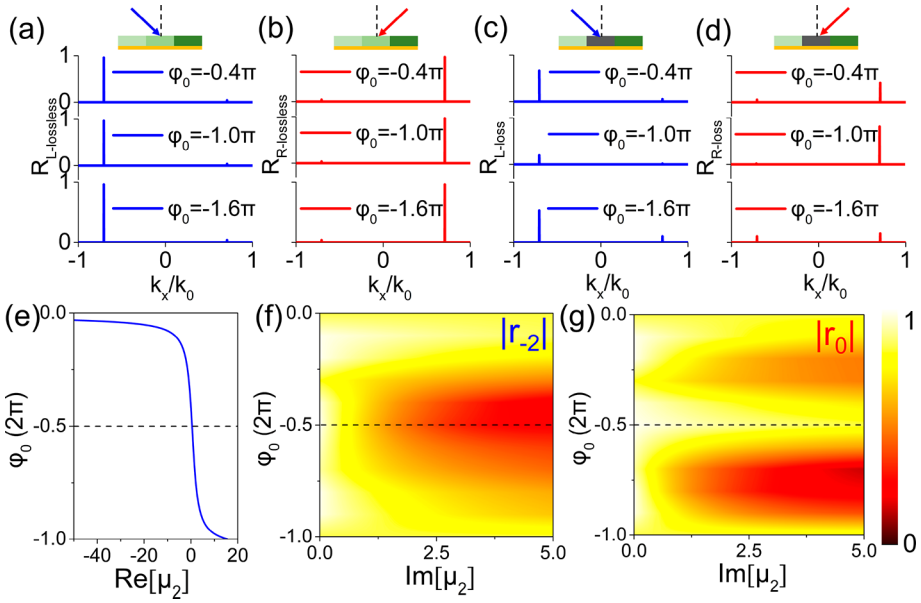

Figure 2. Theoretical demonstration of the angular-asymmetrical scattering features with loss for the EM non-Hermitian metasurface at the wavelength of 1550 nm. The two-port metasurface based on EM is designed with 100 nm thickness and backed up with a mirror. The width P of the tri-meta-atom supercell is about 1096 nm. The local reflective phases of the three subunits in the supercell can be supposed as $\varphi_0 - 2\pi/3$, φ_0, and $\varphi_0 + 2\pi/3$, where φ_0 acts as the reference phase. Different φ_0 correspond to different EM metasurfaces. Normalized scattering intensities of the (a, b) lossless and (c, d) lossy EM metasurfaces calculated by MET when φ_0 is designed at -0.4π, -1.0π, and -1.6π, respectively, for the incident waves from (a, c) the left port and (b, d) the right port. (e) Reflection phase φ_0 versus the effective permeability μ_2 as $\theta_i = 45°$ for the homogeneous metasurface. So the effective dielectric parameters of the three subunits can be retrieved from the database when φ_0 is fixed. Retro-reflection amplitudes of (f) r_{-2} and (g) r_0 as functions of φ_0 and Im[μ_2] for the EM metasurface, respectively.

(right) port, + (−) represents the parallel wave vector of the propagating wave k_x along the x positive (negative) direction, and Ψ_+ (respectively Ψ_-) is the amplitude of the propagating mode with $k_x > 0$ (respectively $k_x < 0$). By a simple analysis, the amplitude Ψ_+^L/Ψ_-^R of the incident wave and the amplitude Ψ_-^L/Ψ_+^R of the scattering wave can build a quantitative relationship by the scattering matrix $\boldsymbol{S}$:

$$\begin{bmatrix} \Psi_+^R \\ \Psi_-^L \end{bmatrix} = \boldsymbol{S} \begin{bmatrix} \Psi_+^L \\ \Psi_-^R \end{bmatrix} = \begin{bmatrix} r_{-1}^L & r_0^R \\ r_{-2}^L & r_{-1}^R \end{bmatrix} \begin{bmatrix} \Psi_+^L \\ \Psi_-^R \end{bmatrix} \tag{2}$$

where r_{-2}^L and r_0^R are the retro-reflection coefficients for the incident waves from the left and right port, respectively; r_{-1}^L and r_{-1}^R are the specular reflection coefficients for the incident waves from the left and right port, respectively, which are identical due to reciprocity. For convenience, the reflection coefficients r_0^R, r_{-2}^L, r_{-1}^L, and r_{-1}^R are simplified as r_0, r_{-2}, and r_{-1} hereafter.

In this work, an EP solution can be achieved on the EM metasurface [$\varepsilon_1 = 8$, $\varepsilon_2 = \varepsilon_3 = 1$; $\mu_1 = 0.8$, $\mu_2 = 0.5$, $\mu_3 = -3.1$] (where [ε_1, ε_2, ε_3] and [μ_1, μ_2, μ_3] represent the permittivities and permeabilities of the three subunits, respectively) in parameter space. When a loss (represented by the imaginary part Im[μ] of μ) is introduced into one subunit (e.g., subunit 2 with Im[μ_2] ≠ 0), an angular-asymmetric scattering feature depending on adjusted loss can be observed. For the periodic inhomogeneous metasurface, the mode-expansion theory (MET) can allow the quantitative analysis of the reflection coefficient of every scattering channel.[3,49] In Figure 1(f), the retro-reflection port shows an asymmetric evolution with Im[μ_2] increasing, where the amplitude of r_{-2} obviously decreases first and then increases, while the amplitude of r_0 is stable around 0.73. Especially, the r_{-2} equals 0 when Im[μ_2] = 2.49, which indicates that the extraordinary retro-reflection from the left port is completely suppressed. In the perspective of $\boldsymbol{S}$ matrix, the eigenvalues $E_\pm = r_{-1} \pm \sqrt{r_0 r_{-2}}$ will coalesce when one of the retroreflective coefficients r_0 and r_{-2} is equal to 0. Figure 1(g) shows the evolution trajectories of the calculated eigenvalues $E_\pm$ of the $\boldsymbol{S}$ matrix with the increase of Im[μ_2] (i.e., along the directions of the red and blue arrows). Obviously, an EP appears in the complex eigenvalue space when the two eigenvalues $E_\pm$ coalesce at Im[μ_2] = 2.49 (where $r_{-2} = 0$). To further demonstrate the non-Hermitian metasurface at the EP, we employ the finite element method (FEM) simulations to calculate the scattering field for the incident waves from two ports, respectively. As shown in Figure 1(d) and (e), the retro-reflection mode is indeed completely suppressed for the left port while still keeping a relatively high intensity for the right.

Here we further show the details of achieving an EP solution for the non-Hermitian metasurface in parameter space. The local reflective phases of the three subunits in the supercell can be supposed as $\varphi_0 - \Delta\varphi$, φ_0, and $\varphi_0 + \Delta\varphi$, where $\Delta\varphi = 2\pi/3$ and φ_0 acts as the reference phase. Then, the effective dielectric parameters of the three subunits can be retrieved from the EM model when φ_0 is fixed (see Figure 2(e) and Section 1 of the Supporting Information). Here, three different metasurfaces based on the EM are chosen to explore when φ_0, as an illustrating example but without losing any generality, is -0.4π, $-\pi$, and -1.6π. The normalized scattering intensities versus k_x are calculated by MET for the incident waves from the left (see Figure 2(a)) and right (see Figure 2(b)), respectively. Obviously, different metasurfaces (corresponding to different φ_0) have the same scattering features once the phase gradient is fixed. Interestingly, this situation will be changed when the loss is introduced. As shown in Figure 2(c)

https://dx.doi.org/10.1021/acsphotonics.0c01440
ACS Photonics 2020, 7, 3321−3327

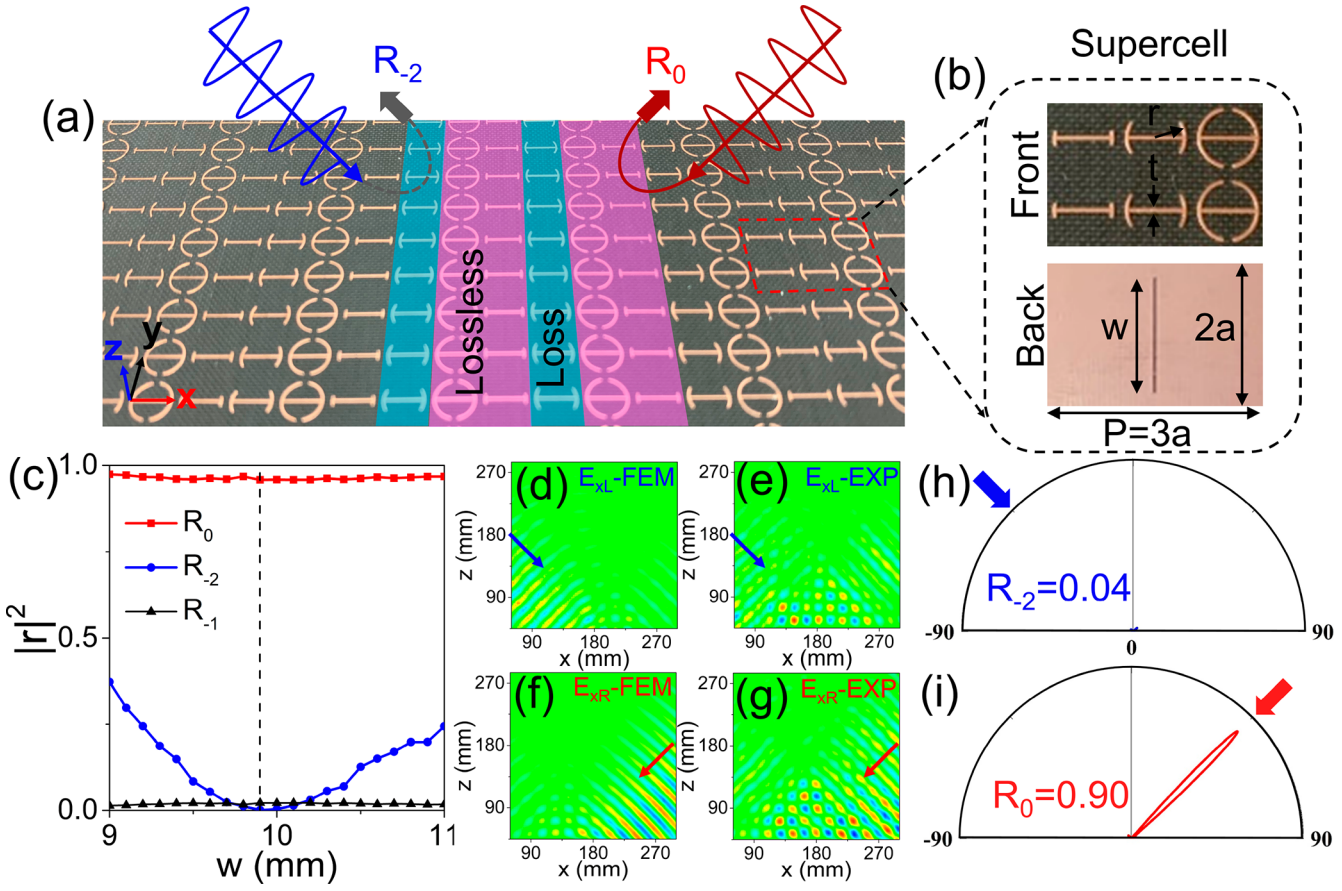

Figure 3. Experimental demonstration of unidirectional retro-reflection for the real non-Hermitian metasurface at 11.8 GHz. (a) Picture of the fabricated non-Hermitian metasurface, consisting of loss and lossless regions, schematically showing extremely asymmetric retro-reflection at the EP. (b) Supercell of the real non-Hermitian metasurface consists of three subunits (with α = 20°, 115°, 152°) composed by a 3-mm-thick dielectric layer (ε_r = 3) sandwiched between the metallic sheet and the metal H-shaped ring layer (r = 3.5 mm, t = 0.2 mm). The lossless subunits consist of two identical meta-atoms with the fixed size ($a \times a$ mm^2, a = 6 mm), and the leaky loss is introduced into subunit 2 by a 0.2-mm-width slit with a length of w = 9.9 mm. Here, all of the thicknesses of the metal films are 36 μm. (c) FEM-simulated reflectivities R_0, R_{-2}, and R_{-1} versus w for the non-Hermitian metasurface (with infinite size). (d, f) FEM-simulated and (e, g) experimental near-field E_x pattern of the non-Hermitian metasurface (with real size) on the xz plane for the incident waves from (d, e) the left port and (f, g) the right port. FDTD-simulated far-field intensity of the non-Hermitian metasurface (with real size) versus the detected angle for the incident waves from (h) the left port and (i) the right port, respectively.

and (d), these scattering characteristics become seemingly random when a loss (e.g., Im[μ_2] = 2) is introduced into the subunit 2 (of which the site chosen is not special due to the periodicity of the supercell and the loop of φ_0 within 2π). Furthermore, the calculated retro-reflection amplitudes $|r_{-2}|$ and $|r_0|$ versus Im[μ_2] and φ_0 for the corresponding metasurfaces are shown in Figure 2(f) and (g). Obviously, the retro-reflection features for the incident waves from the left port and right port become asymmetric as the loss is introduced into the EM metasurface. Especially around $\varphi_0 = -\pi$, $|r_{-2}|$ is gradually suppressed with Im[μ_2] increasing, while $|r_0|$ remains stable in this region, which shows the expected angular-asymmetric retro-reflection suppression. After a slight adjustment for the subunit 1 of the EM model at $\varphi_0 = -\pi$, an EP solution of the non-Hermitian metasurface [ε_1 = 8, $\varepsilon_2 = \varepsilon_3$ = 1; μ_1 = 0.8, μ_2 = 0.5 + i2.49, μ_3 = −3.1] based on EM can be fixed (see Figure S3 in the Supporting Information).

As a proof of concept, a Janus retro-reflective measurface at EP has been experimentally demonstrated at 11.8 GHz. Figure 3(a) shows the partial picture of the sample (with 340 × 360 mm^2 size), consisting of lossless and lossy regions, of which the supercell constructed by three subunits (α_1 = 20°, α_2 = 115°, α_3 = 152°, see Figure S5 in the Supporting Information) is composed of the H-shaped metal ring (r = 3.5 mm, t = 0.2 mm) and a rectangular dielectric spacer (ε_r = 3, a = 6 mm) on a metal base, as shown in Figure 3(b). The finite difference time domain (FDTD) method shows the reflection phase versus α at θ_i = 45° (see Figure 1(c) and Figure S5(a) in the Supporting Information). A leaky loss is introduced into subunit 2 by a 0.2-mm-width slit in the metal base. The length w of the slit is further adjusted to change the effective loss of subunit 2. Figure 3(c) displays the FEM-simulated scattering intensities R_0, R_{-2}, and R_{-1} versus w for the non-Hermitian metasurface with infinite size (i.e., periodic boundary condition along the x direction) where an asymmetric retro-reflection is observed. Especially, the retro-reflection mode from the left port is completely suppressed (R_{-2} = 0) when w = 9.9 mm, while the retro-reflection efficiency (R_0) from the right port still remains around 96%. Interestingly, the ordinary specular reflection R_{-1} stays naturally weak (~2%) in the whole region, which may be due to the stable phase as the loss changed for the real structure (see Figure S6 in the Supporting Information).

https://dx.doi.org/10.1021/acsphotonics.0c01440
ACS Photonics 2020, 7, 3321−3327

To show the exotic performance of the non-Hermitian metasurface at the EP, the near-field and far-field scattering responses are characterized in microwave experiments. In experiments, a horn antenna is used as the incident source is placed 1 m away from the sample at specified angles of incidence. For near-field experiments, a monopole antenna tip used as the receiver along the the x direction is sweeping in the xz plane (y = 0) to measure the E_x field distribution. For far-field experiments, another horn antenna used as the receiver was placed 3 m away from the sample and could be freely moved around the sample to receive the far-field scattering signals. Both the incident horn and the receiver are connected to a vector network analyzer (Agilent E8362CPNA) so that the receiving signals can contain both amplitude and phase information (details in Section 3 of the Supporting Information). The scattering field distributions (E_x) via the FEM simulation are shown in Figure 3(d) and (f), and the experimental measurements for $\theta_i = 45°$ and $\theta_i = -45°$ are shown in Figure 3(e) and (g), respectively, which show a good agreement on the distinct contrast of the two retro-reflection fields. Of course, strictly, there is still a little difference especially for the specular reflection mode, which may result from sample error (i.e., the etch tolerance is 1.5 mil and the permittivity tolerance of the used F4B material is 0.03) and the incident source error. For the far-field measurements, the angular distributions of the scattering field at $\theta_i = \pm 45°$ cannot be precisely measured due to the axial overlapping between the incident horn and the receiving horn (see Figure S7(a) in the Supporting Information). Therefore, we measure the far-field distributions at $\theta_i = \pm 30°$ and $\theta_i = \pm 60°$ to indirectly demonstrate our design, which matches well with the expected results (see Figure S7(d)−(g) in the Supporting Information). Furthermore, we characterize the far-field scattering features of the sample with real size at $\theta_i = \pm 45°$ with FDTD simulations as shown in Figure 3(h) and (i). As expected, the retro-reflection mode from the left port is nearly completely suppressed (the efficiency is ∼4%), while the retro-reflection efficiency reaches 90% for the right port. The extremely angular asymmetry hardly can be realized on traditional lossless metasurfaces or a metagrating.[50] Moreover, we also note that such an asymmetric scattering effect can exist within a certain range of incidence angle and frequency band for the non-Hermitian metasurface based on the real structure at the EP (see Figures S7(h) and S8 in the Supporting Information).

CONCLUSION

To summarize, we proposed a non-Hermitian metasurface that combines the classical phase-gradient approach with modulated loss. The passive system can achieve an EP by balancing lossless and lossy regions. The extremely angular-asymmetric scattering suppression emerging at the EP has been theoretically and experimentally demonstrated. Our investigations provide a new perspective to design an asymmetric optics system and further inspire the exploration of a more complex EP or higher-order EP solution for metasurfaces.

ASSOCIATED CONTENT

Supporting Information

The Supporting Information is available free of charge at https://pubs.acs.org/doi/10.1021/acsphotonics.0c01440.

Effective medium model for reflection-type homogeneous metasurfaces, EM solution of the non-Hermitian metasurface at the EP in parameter space, a real solution of the non-Hermitian metasurface at the EP based on real structure, details of numerical simulations (PDF)

AUTHOR INFORMATION

Corresponding Authors

Ying Li − *SZU-NUS Collaborative Innovation Center for Optoelectronic Science & Technology, International Collaborative Laboratory of 2D Materials for Optoelectronics Science and Technology of Ministry of Education, Institute of Microscale Optoelectronics, Shenzhen University, Shenzhen 518060, China*; Email: queenly@vip.sina.com

Cheng-Wei Qiu − *Department of Electrical and Computer Engineering, National University of Singapore, Singapore 117583 Singapore*; orcid.org/0000-0002-6605-500X; Email: chengwei.qiu@nus.edu.sg

Authors

Shaohua Dong − *SZU-NUS Collaborative Innovation Center for Optoelectronic Science & Technology, International Collaborative Laboratory of 2D Materials for Optoelectronics Science and Technology of Ministry of Education, Institute of Microscale Optoelectronics, Shenzhen University, Shenzhen 518060, China; Department of Electrical and Computer Engineering, National University of Singapore, Singapore 117583 Singapore*

Guangwei Hu − *Department of Electrical and Computer Engineering, National University of Singapore, Singapore 117583 Singapore*; orcid.org/0000-0002-3023-9632

Qiang Wang − *State Key Laboratory of Millimeter Waves, School of Information Science and Engineering, Southeast University, Nanjing 210096, China*

Yuxiang Jia − *Department of Basic Sciences, Air Force Engineering University, Xian 710051, China*

Qing Zhang − *Department of Electrical and Computer Engineering, National University of Singapore, Singapore 117583 Singapore*

Guangtao Cao − *Department of Electrical and Computer Engineering, National University of Singapore, Singapore 117583 Singapore*

Jiafu Wang − *Department of Basic Sciences, Air Force Engineering University, Xian 710051, China*

Shuqing Chen − *SZU-NUS Collaborative Innovation Center for Optoelectronic Science & Technology, International Collaborative Laboratory of 2D Materials for Optoelectronics Science and Technology of Ministry of Education, Institute of Microscale Optoelectronics, Shenzhen University, Shenzhen 518060, China*; orcid.org/0000-0002-2321-4760

Dianyuan Fan − *SZU-NUS Collaborative Innovation Center for Optoelectronic Science & Technology, International Collaborative Laboratory of 2D Materials for Optoelectronics Science and Technology of Ministry of Education, Institute of Microscale Optoelectronics, Shenzhen University, Shenzhen 518060, China*

Weixiang Jiang − *State Key Laboratory of Millimeter Waves, School of Information Science and Engineering, Southeast University, Nanjing 210096, China*; orcid.org/0000-0002-3122-5937

Andrea Alù − *Photonics Initiative, Advanced Science Research Center and Physics Program, Graduate Center, City University of New York, New York, New York 10010, United States*

https://dx.doi.org/10.1021/acsphotonics.0c01440
ACS Photonics 2020, 7, 3321−3327

Complete contact information is available at:
https://pubs.acs.org/10.1021/acsphotonics.0c01440

Notes

The authors declare no competing financial interest.

■ ACKNOWLEDGMENTS

This project was supported by the A*STAR Pharos Program (grant number 15270 00014, with project number R-263-000-B91-305), the National Research Foundation, Prime Minister's Office, Singapore, under its Competitive Research Program (CRP award number NRFCRP 15-2015-03), and the Air Force Office of Scientific Research.

■ REFERENCES

(1) Yu, N.; Genevet, P.; Kats, M. A.; Aieta, F.; Tetienne, J. P.; Capasso, F.; Gaburro, Z. Light propagation with phase discontinuities: generalized laws of reflection and refraction. *Science* **2011**, *334*, 333.
(2) Alexander, V.; Kildishev, A.; Boltasseva; Shalaev, V. M. Planar photonics with metasurfaces. *Science* **2013**, *339*, 1232009.
(3) Sun, S.; He, Q.; Xiao, S.; et al. Gradient-index meta-surfaces as a bridge linking propagating waves and surface waves. *Nat. Mater.* **2012**, *11*, 426.
(4) Yin, X.; Ye, Z.; Rho, J.; Wang, Y.; Zhang, X. Photonic spin Hall effect at metasurfaces. *Science* **2013**, *339*, 1405.
(5) Zhou, J.; Qian, H.; Hu, G.; Luo, H.; Wen, S.; Liu, Z. Broadband Photonic Spin Hall Meta-Lens. *ACS Nano* **2018**, *12*, 82.
(6) Hu, G.; Hong, X.; Wang, K.; et al. Coherent steering of nonlinear chiral valley photons with a synthetic Au-WS2 metasurface. *Nat. Photonics* **2019**, *13*, 467.
(7) Arbabi, A.; Horie, Y.; Ball, A. J.; Bagheri, M.; Faraon, A. Subwavelength-thick lenses with high numerical apertures and large efficiency based on high-contrast transmitarrays. *Nat. Commun.* **2015**, *6*, 1.
(8) Khorasaninejad, M.; Chen, W. T.; Devlin, R. C.; Oh, J.; Zhu, A. Y.; Capasso, F. Metalenses at visible wavelengths: Diffraction-limited focusing and subwavelength resolution imaging. *Science* **2016**, *352*, 1190.
(9) Huang, L.; Chen, X.; Mühlenbernd, H.; et al. Three-dimensional optical holography using a plasmonic metasurface. *Nat. Commun.* **2013**, *4*, 1.
(10) Zheng, G.; Mühlenbernd, H.; Kenney, M.; Li, G.; Zentgraf, T.; Zhang, S. Metasurface holograms reaching 80% efficiency. *Nat. Nanotechnol.* **2015**, *10*, 308.
(11) Chen, W. T.; Yang, K. Y.; Wang, C. M.; et al. High-efficiency broadband meta-hologram with polarization-controlled dual images. *Nano Lett.* **2014**, *14*, 225.
(12) Yu, P.; Li, J.; Zhang, S.; et al. Dynamic Janus metasurfaces in the visible spectral region. *Nano Lett.* **2018**, *18*, 4584.
(13) Chen, K.; Ding, G.; Hu, G.; et al. Directional Janus Metasurface. *Adv. Mater.* **2020**, *32*, 1906352.
(14) Xu, H. X.; Hu, G.; Jiang, M.; et al. Wavevector and frequency multiplexing performed by a Spin-decoupled multichannel metasurface. *Adv. Mater. Technol.* **2020**, *5*, 1900710.
(15) Sun, S.; Yang, K. Y.; Wang, C. M.; et al. High-efficiency broadband anomalous reflection by gradient meta-surfaces. *Nano Lett.* **2012**, *12*, 6223.
(16) Wang, X.; Díaz-Rubio, A.; Asadchy, V. S.; Ptitcyn, G.; Generalov, A. A.; Ala-Laurinaho, J.; Tretyakov, S. A. Extreme asymmetry in metasurfaces via evanescent fields engineering: angular-asymmetric absorption. *Phys. Rev. Lett.* **2018**, *121*, 256802.
(17) Dong, S.; Zhang, Y.; Guo, H.; Duan, J.; Guan, F.; He, Q.; Zhao, H.; Zhou, L.; Sun, S. Highly efficient wave-front reshaping of surface waves with dielectric metawalls. *Phys. Rev. Appl.* **2018**, *9*, No. 014032.
(18) Dong, S.; Zhang, Q.; Cao, G.; et al. On-chip trans-dimensional plasmonic router. *Nanophotonics* **2020**, *9*, 3357.
(19) Bender, C. M.; Boettcher, S. Real spectra in non-Hermitian Hamiltonians having PT symmetry. *Phys. Rev. Lett.* **1998**, *80*, 5243.
(20) Bender, C. M. Making sense of non-Hermitian Hamiltonians. *Rep. Prog. Phys.* **2007**, *70*, 947.
(21) Bender, C. M.; Brody, D. C.; Jones, H. F. Complex extension of quantum mechanics. *Phys. Rev. Lett.* **2002**, *89*, 270401.
(22) El-Ganainy, R.; Makris, K. G.; Christodoulides, D. N.; Musslimani, Z. H. Theory of coupled optical PT-symmetric structures. *Opt. Lett.* **2007**, *32*, 2632.
(23) Zhu, X.; Ramezani, H.; Shi, C.; Zhu, J.; Zhang, X. PT-symmetric acoustics. *Phys. Rev. X* **2014**, *4*, No. 031042.
(24) Wang, X.; Fang, X.; Mao, D.; Jing, Y.; Li, Y. Extremely asymmetrical acoustic metasurface mirror at the exceptional point. *Phys. Rev. Lett.* **2019**, *123*, 214302.
(25) Schindler, J.; Li, A.; Zheng, M. C.; Ellis, F. M.; Kottos, T. Experimental study of active LRC circuits with PT symmetries. *Phys. Rev. A: At., Mol., Opt. Phys.* **2011**, *84*, No. 040101.
(26) Li, Y.; Peng, Y. G.; Han, L.; et al. Anti-parity-time symmetry in diffusive systems. *Science* **2019**, *364*, 170.
(27) Guo, A.; Salamo, G. J.; Duchesne, D.; et al. Observation of PT-symmetry breaking in complex optical potentials. *Phys. Rev. Lett.* **2009**, *103*, No. 093902.
(28) Makris, K. G.; El-Ganainy, R.; Christodoulides, D. N.; Musslimani, Z. H. Beam dynamics in PT-symmetric optical lattices. *Phys. Rev. Lett.* **2008**, *100*, 103904.
(29) Klaiman, S.; Guenther, U.; Moiseyev, N. Visualization of branch points in PT symmetric waveguides. *Phys. Rev. Lett.* **2008**, *101*, No. 080402.
(30) Longhi, S. Bloch oscillations in complex crystals with PT symmetry. *Phys. Rev. Lett.* **2009**, *103*, 123601.
(31) Zheng, M. C.; Christodoulides, D. N.; Fleischmann, R.; Kottos, T. PT optical lattices and universality in beam dynamics. *Phys. Rev. A: At., Mol., Opt. Phys.* **2010**, *82*, No. 010103R.
(32) Chong, Y. D.; Ge, L.; Stone, A. D. PT-symmetry breaking and laser-absorber modes in optical scattering systems. *Phys. Rev. Lett.* **2011**, *106*, No. 093902.
(33) Feng, L.; Wong, Z. J.; Ma, R. M.; Wang, Y.; Zhang, X. Single-mode laser by parity-time symmetry breaking. *Science* **2014**, *346*, 972.
(34) Monticone, F.; Valagiannopoulos, C. A.; Alù, A. Parity-time symmetric nonlocal metasurfaces: all-angle negative refraction and volumetric imaging. *Phys. Rev. X* **2016**, *6*, No. 041018.
(35) Feng, L.; El-Ganainy, R.; Ge, L. Non-Hermitian photonics based on parity-time symmetry. *Nat. Photonics* **2017**, *11*, 752.
(36) Özdemir, Ş. K.; Rotter, S.; Nori, F.; Yang, L. Parity-time symmetry and exceptional points in photonics. *Nat. Mater.* **2019**, *18*, 783.
(37) Miri, M. A.; Alù, A. Exceptional points in optics and photonics. *Science* **2019**, *363*, No. eaar7709.
(38) Feng, L.; Xu, Y. L.; Fegadolli, W. S.; Lu, M. H.; Oliveira, J. E.; Almeida, V. R.; Chen, Y. F.; Scherer, A. Experimental demonstration of a unidirectional reflectionless parity-time metamaterial at optical frequencies. *Nat. Mater.* **2013**, *12*, 108.
(39) Lawrence, M.; Xu, N.; Zhang, X.; Cong, L.; Han, J.; Zhang, W.; Zhang, S. Manifestation of PT symmetry breaking in polarization space with terahertz metasurfaces. *Phys. Rev. Lett.* **2014**, *113*, No. 093901.
(40) Park, S. H.; Leea, S.-G.; Baek, S.; Ha, T.; Lee, S.; Min, B.; Zhang, S.; Lawrence, M.; Kim, T.-T. Observation of an exceptional point in a non-Hermitian metasurface. *Nanophotonics* **2020**, *9*, 1031.
(41) Chen, P. Y.; Sakhdari, M.; Hajizadegan, M.; Cui, Q.; Cheng, M. M. C.; El-Ganainy, R.; Alù, A. Generalized parity−time symmetry condition for enhanced sensor telemetry. *Nat. Electron.* **2018**, *1*, 297.
(42) Sun, Y.; Tan, W.; Li, H.; Li, J.; Chen, H. Experimental Demonstration of a Coherent Perfect Absorber with PT Phase Transition. *Phys. Rev. Lett.* **2014**, *112*, 143903.
(43) Ye, Z.; Farhat, M.; Chen, P. Y. Tunability and switching of Fano and Lorentz resonances in PTX-symmetric electronic systems. *Appl. Phys. Lett.* **2020**, *117*, No. 031101.

(44) Lee, S. B.; Yang, J.; Moon, S.; et al. Observation of an exceptional point in a chaotic optical microcavity. *Phys. Rev. Lett.* **2009**, *103*, 134101.
(45) Choi, Y.; Kang, S.; Lim, S.; Kim, W.; Kim, J. R.; Lee, J. H.; An, K. Quasieigenstate coalescence in an atom-cavity quantum composite. *Phys. Rev. Lett.* **2010**, *104*, 153601.
(46) Feng, L.; Zhu, X.; Yang, S.; et al. Demonstration of a large-scale optical exceptional point structure. *Opt. Express* **2014**, *22*, 1760.
(47) Huang, Y.; Shen, Y.; Min, C.; Fan, S.; Veronis, G. Unidirectional reflectionless light propagation at exceptional points. *Nanophotonics* **2017**, *6*, 977.
(48) Hao, J. M.; Zhou, L.; Chan, C. T. An effective-medium model for high-impedance surfaces. *Appl. Phys. A: Mater. Sci. Process.* **2007**, *87*, 281.
(49) Xiao, S.; He, Q.; Qu, C.; Li, X.; Sun, S.; Zhou, L. Mode-expansion theory for inhomogeneous meta-surfaces. *Opt. Express* **2013**, *21*, 27219.
(50) Ra'di, Y.; Sounas, D. L.; Alù, A. Metagratings: Beyond the limits of graded metasurfaces for wave front control. *Phys. Rev. Lett.* **2017**, *119*, No. 067404.

https://dx.doi.org/10.1021/acsphotonics.0c01440
ACS Photonics 2020, 7, 3321−3327